Determination of spin Hall angle and spin diffusion length in β-phase-dominated tantalum

R. Yu,[1] B. F. Miao,[1,2] L. Sun,[1,2] Q. Liu,[1] J. Du,[1,2] P. Omelchenko,[3] B. Heinrich,[3] Mingzhong Wu,[4] and H. F. Ding[1,2,*]

[1]*National Laboratory of Solid State Microstructures and Department of Physics, Nanjing University, 22 Hankou Road, Nanjing 210093, People's Republic of China*

[2]*Collaborative Innovation Center of Advanced Microstructures, Nanjing University, 22 Hankou Road, Nanjing 210093, People's Republic of China*

[3]*Department of Physics, Simon Fraser University, 8888 University Dr, Burnaby, British Columbia V5A 1S6, Canada*

[4]*Department of Physics, Colorado State University, Fort Collins, Colorado 80523, USA*

(Received 16 February 2018; published 23 July 2018)

The dc spin-to-charge conversions of tantalum (Ta) in Ta/$Co_{40}Fe_{40}B_{20}$ bilayer structures are investigated utilizing spin pumping and inverse spin Hall effects (ISHE). From Ta thickness (t_{Ta})-dependent resistivity and x-ray diffraction measurements, we found that Ta films, below 30 nm in thickness, are β-phase dominated. The damping enhancement shows a fast increase with t_{Ta} when $t_{Ta} < 1$ nm and reaches a saturation value at $\sim$1.5 nm. The ISHE induced charge voltages have opposite signs for Ta and Pt. From t_{Ta}-dependent spin pumping produced ISHE voltage and precession angle measurements, the normalized spin-charge conversion signal is found to increase with t_{Ta} and saturate at $\sim$15 nm. Our findings can be understood with a recently developed theory [Phys. Rev. Lett. **114**, 126602 (2015)], which includes spin backflow and a spin loss at the interface. With a fitted spin loss factor of 0.02 ± 0.02, we extract the spin Hall angle and spin diffusion length of high resistivity Ta to be $\theta_{SH} = -0.0062 \pm 0.001$ and $\lambda_{sd} = 5.1 \pm 0.6$ nm, respectively.

DOI: 10.1103/PhysRevMaterials.2.074406

Spintronics, a paradigm of electronics based on the spin degree of freedom of the electron, has attracted increasing attention due to the advantages of being nonvolatile, reduced power dissipation, and increased storage density as compared to traditional electronics devices [1–5]. Spintronics initially emerged as the utilization of spin-polarized currents. Recently, spintronics entered a new stage: exploration of pure spin currents. In comparison with spin-polarized currents, pure spin currents are of more interest since they are accompanied by neither net charge currents nor stray Oersted fields and can therefore carry information with minimal power dissipation [6,7]. Thus, it can be anticipated that pure spin currents will play a crucial role in future spin-based electronic devices. To integrate with current technology, which is mainly charge based, pure spin signals need to interconvert efficiently with charge signals. The spin and charge currents can interconvert to each other in nonmagnetic materials by means of the spin Hall effect (SHE) or the inverse spin Hall effect (ISHE) [5,8]. The conversion efficiency, typically characterized by the spin Hall angle (θ_{SH}), is thus one of the key parameters for spintronics applications.

Various methods have been utilized to generate pure spin currents and estimate θ_{SH}, such as nonlocal spin injection [9], ferromagnetic resonance (FMR) based spin pumping [10–13], thermal spin injection [14], and spin torque FMR [15], etc. Among them, spin pumping is commonly used in transition metals since their interfaces can be better characterized and be free from the impedance mismatching issue [7,16]. Upon the microwave excitation, the magnetic moments in a ferromagnet (F) precess and inject a pure spin current $\boldsymbol{J_S}$ into an adjacent normal metal (N), and $\boldsymbol{J_S}$ is further converted into an electrical current $\boldsymbol{J_C}$ via the ISHE through $\boldsymbol{J_C} = (2e/\hbar)\theta_{SH}\boldsymbol{J_S} \times \boldsymbol{\sigma}$, where $\boldsymbol{\sigma}$ denotes the spin-polarization direction of $\boldsymbol{J_S}$ and $\hbar$ is the reduced Planck constant. Generally, large θ_{SH} is believed to exist in 4*d* and 5*d* transition metals [17]. Comparable θ_{SH} values were also reported recently in alloys like CuBi [18], Permalloy [14], and 3*d* transition metals such as Cr and Ni [19]. Among those materials, β-Ta is of special interest as it has been predicted to have a large and negative θ_{SH} [17]. A subsequent experiment also showed that β-Ta can serve as a material for high efficiency magnetization switching [20]. Thus, the study of θ_{SH} in β-Ta attracts great interest. Previously reported θ_{SH} of Ta vary greatly, ranging from -0.0037 to -0.15 [20–28]. Therefore, a systematical study to accurately determine the actual θ_{SH} is highly desired.

The discrepancy of the previously measured θ_{SH} may originate for the following reasons. First, during the spin pumping experiment, the detected voltage signal can include two components: the ISHE voltage (V_{ISHE}^{SP}) and an unwanted signal which is typically related to anisotropic magnetoresistance (AMR), V_{AMR} [10,12,29]. V_{ISHE}^{SP} has a symmetrical Lorentzian line shape centered at the FMR field, H_r. In contrast, V_{AMR} can have both the antisymmetrical and symmetrical Lorentzian line-shape components also centered at H_r [29–32]. The presence of V_{AMR} thus can influence the measurement of V_{ISHE}^{SP}. Therefore, the careful separation of these two signals is necessary. Second, θ_{SH} by definition is the ratio of the spin to charge current before and after the conversion. Thus, it is important to measure both spin and charge signals instead of the charge signal alone. Most of the studies, however, assumed that the injected spin current has no dependence on

*Corresponding author: hfding@nju.edu.cn

the thickness of the adjacent nonmagnetic film. It was recently reported that the precession angle, to which the spin current is proportional, can depend on the thickness of the nonmagnetic layer even if constant microwave power used [13]. Therefore, it is also important to measure the precession angles for each individual sample [13,32,33]. Third, the measurement of θ_{SH} is also connected with another important material parameter, the spin diffusion length (λ_{sd}). λ_{sd} determines the length scale of spin current transport [34] and defines the effective thickness for the spin-to-charge conversion. Thus, a careful thickness-dependent study is needed to quantify both θ_{SH} and λ_{sd}. Fourth, recent studies showed that the spin current may suffer a loss when flowing across an interface and can therefore influence the determination of θ_{SH} and λ_{sd} [34–37]. So, a careful characterization of the interface effect on the spin transport is also necessary.

In this study, we present a systematic study of θ_{SH} and λ_{sd} for β-phase dominated Ta by taking into account all of the above-mentioned issues carefully. We used $Ta/Co_{40}Fe_{40}B_{20}$ (Ta/CoFeB) bilayer samples. Using a combination of thickness-dependent resistivity and x-ray diffraction (XRD) measurements, we identified that the Ta films are mainly in β phase when the film thickness is 30 nm and less. Through the measurement of the spin pumping induced ISHE (SP-ISHE) signal at specially chosen geometry, we excluded the AMR signal and obtained the pure ISHE signal [12,29]. With microwave photoresistance measurements, the actual pumped spin current was characterized for each individual sample by measuring the precession angles. To account for spin current transport at the interface we measured t_{Ta} dependence ($t_{Ta} < 2$ nm) of enhanced interface damping; the data were analyzed by the recently developed model in Refs. [36,37], allowing one to estimate the spin loss at the interface. With all these efforts, we found $\theta_{SH} = -0.0062 \pm 0.001$ and $\lambda_{sd} = 5.1 \pm 0.6$ nm for β-phase dominated Ta.

The Ta/CoFeB bilayers were grown on GaAs (001) substrate by dc magnetron sputtering deposition at room temperature. The base pressure of the chamber is 2×10^{-5} Pa. Prior to the growth, the substrates are thoroughly rinsed sequentially with acetone, ethanol, and deionized water in an ultrasonic water bath (100 W). During the growth, the Ar pressure is maintained at 0.3 Pa. The growth conditions for the deposition of Ta are 0.046 A for the current and 348 V for the applied voltage. The Ta growth rate is calibrated by XRD to be ~0.111 nm/s. Immediately after the growth of the Ta film, we grow the CoFeB film on top of the Ta film in the same chamber with the conditions of 0.06 A for the current and 396 V for the voltage. The calibrated growth rate for CoFeB is ~0.176 nm/s. The distance between the target and the substrate is fixed at ~65 mm for both Ta and CoFeB. The bilayers are patterned into stripes with the width of $w = 20\ \mu m$ and length of $L = 1820\ \mu m$ through photolithography and lift-off techniques. Figure 1(a) shows the sketch of the device used for the measurements. The light blue rectangles are the signal line (S) and the ground lines (G) of a coplanar waveguide (CPW). The purple long stripe represents the sample that is placed in the center between S and G lines. In this structure, the microwave magnetic field $\vec{h}_{rf}$ is mainly perpendicular to the sample plane and along the z direction [29]. A network analyzer with the variable frequency f in the range of 20

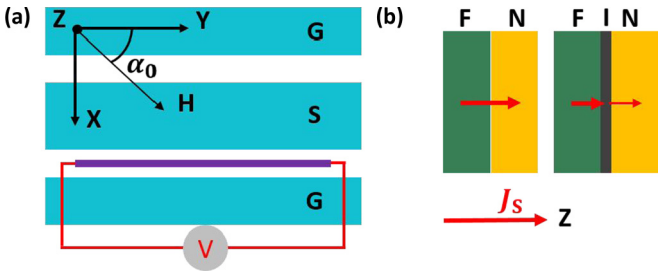

FIG. 1. (a) Schematic illustration of the experimental setup for the spin pumping induced ISHE voltage measurement. The Ta/CoFeB bilayer is placed in the middle of the gap between the ground (G) and signal (S) lines of a coplanar waveguide. (b) Schematic illustration of spin current transmission across the interface (I) between ferromagnetic (F) and normal (N) layers without considering interface spin loss (left) and with the interface spin loss (right).

MHz to 20 GHz was used to generate a microwave power for SP-ISHE and FMR measurements. A rotatable dc magnetic field $\vec{H}$ with tunable magnitude was applied within the sample plane. The angle between $\vec{H}$ and the bilayer stripe, α_0, can be controlled through a servomotor with high accuracy (error margin <0.15°). In the measurements, the resistance of the stripe is measured with the four probes method and the voltage generated by spin pumping is detected as a function of $\vec{H}$ via the two contact bars placed at both ends of the stripes. To increase the signal-to-noise ratio, a lock-in amplifier was used in the configuration of amplitude modulation of the microwave signal with a frequency 51.73 kHz. All the measurements were performed at room temperature. Figure 1(b) shows a schematic illustration of the spin current transport across the interface (black) between ferromagnetic (green) and normal (yellow) layers. On the left, the spin current is transmitted through the interface without any loss. On the right, the spin current suffers an interface spin loss during the transmission, and only a part of the pumped spin current enters the nonmagnetic layer and is further converted into the charge current due to ISHE.

Tantalum has $5d^3 6s^2$ outer shell electrons and is less than half filled in d orbits. Therefore, it is anticipated to have a negative spin Hall angle [17], in contrast to the positive one reported for Pt ($5d^9 6s^1$). Figure 2(a) shows the measured voltage as the function of $\vec{H}$ for both the Pt and Ta layers. The green circles are for Ta (5)/CoFeB (10) (the numbers in parentheses are the layer thicknesses in nm) and the black circle are for Pt (5)/CoFeB (10). The solid red lines are the fits utilizing the symmetric Lorentzian line shape. Both measurements are taken at 8 GHz. In order to eliminate the unwanted V_{AMR}, we followed our previous approach [12,29] and chose two special geometries, i.e., $\alpha_0 = 90°$ and $\alpha_0 = 270°$ (not shown) according to their different dependences on the angle α_0: $V_{ISHE}^{SP} \propto \sin\alpha_0$ and $V_{AMR} \propto \sin 2\alpha_0$. As shown in Fig. 2(a), the experimental data can be fit well by the symmetric Lorentzian line shape (red curves). The signals are inverted for the same sample for $\alpha_0 = 90°$ and $\alpha_0 = 270°$ (not shown). The almost perfect fit with symmetrical Lorentzian line shape and the sign inversion at $\alpha_0 = 90°$ and $\alpha_0 = 270°$ evidence that the measured signals are pure ISHE signals caused by spin pumping. Noticeably, the dc voltage signals

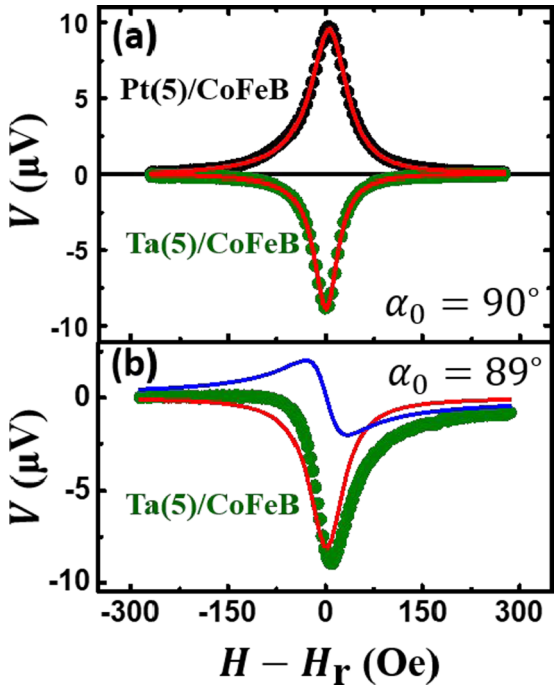

FIG. 2. (a) The measured voltage as the function of the external dc magnetic field, $\vec{H}$. The green solid symbols are for Ta (5)/CoFeB (10) and the black solid symbols are for Pt (5)/CoFeB (10). The data are obtained with $f = 8$ GHz and $\alpha_0 = 90°$. The red lines are the fits utilizing the symmetrical Lorentzian function. (b) The measured voltage as a function of the external dc magnetic field $\vec{H}$ for Ta(5)/CoFeB (10) at $f = 10$ GHz and $\alpha_0 = 89°$. Symbols are the experimental data. The solid red/blue lines are the fits with the symmetrical/antisymmetrical Lorentzian functions, respectively.

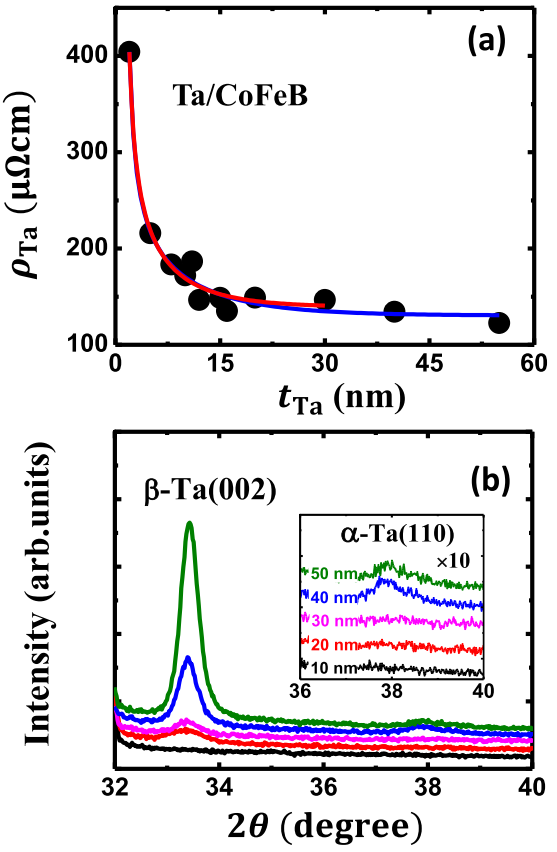

FIG. 3. (a) The Ta thickness-dependent resistivity. Symbols are the experimental data, and the lines is a fit using the Fuchs-Sondheimer model. (b) θ–2θ XRD scan of Ta (10, 20, 30, 40, and 50 nm) films deposited on GaAs substrates. The inset shows the amplified view.

obtained for Ta and Pt are indeed opposite in sign, as predicted theoretically [17].

As mentioned above, the measured $V_{\mathrm{ISHE}}^{\mathrm{SP}}$ in real experiments is often mixed with V_{AMR}. When the angle α_0 is not exactly equal to 90° or 270°, the measured voltage for Ta (5)/CoFeB (10) bilayer can contain both symmetric and antisymmetric signals due to the mixing with V_{AMR}. To illustrate this effect, we show the signal obtained at a slightly tilted angle, $\alpha_0 = 89°$, in Fig. 2(b). Interestingly, the measured voltage is no longer purely symmetrical even though α_0 is only tilted away by 1° from 90°. Our fits yield the antisymmetrical component (solid blue line) to be ∼4 μV, which is ∼40% of ∼9 μV obtained for the symmetrical component (solid red line). We note that a similar effect is also observed by Obstbaum *et al.* [38]. Therefore, ISHE study requires highly accurate alignment of the sample geometry to obtain the pure and noncontaminated ISHE voltage signal.

Ta films grown by sputtering can form two different crystalline phases: the bcc phase (α-Ta) and the tetragonal phase (β-Ta). These two phases were reported to have significantly different resistivity in Ref. [39]. This difference was also confirmed by several experiments [40–42]. Though the exact resistivity depends on the substrate and the growth conditions, it is generally accepted that the resistivity is 15–50 $\mu\Omega$cm for α-Ta and 140–220 $\mu\Omega$cm for β-Ta, respectively. To determine the resistivity of our Ta films, deposited on top of GaAs substrates, we measured the resistance for Ta (t_{Ta}) with t_{Ta} varied in the range of 2–55 nm with four probes method. The results are shown in Fig. 3(a). The t_{Ta}-dependent ρ_{Ta} shows a large value of 400 $\mu\Omega$cm at 2 nm, a fast decrease when $t_{\mathrm{Ta}} < 15$ nm, and a slow decrease for $t_{\mathrm{Ta}} > 15$ nm. To obtain quantitative information, we fit our results with a semiclassical Fuchs-Sondheimer model [43], $\rho_{\mathrm{Ta}} = \rho_0[1 - (\frac{1}{2} + \frac{3\lambda_{\mathrm{mf}}}{4t_{\mathrm{Ta}}})(1 - pe^{-t_{\mathrm{Ta}}\xi/\lambda_{\mathrm{mf}}})e^{-t_{\mathrm{Ta}}/\lambda_{\mathrm{mf}}}]^{-1}$ with $t_{\mathrm{Ta}}/\lambda_{\mathrm{mf}} > 0.1$. In it, ρ_0 represents the bulk resistivity, λ_{mf} stands for the electron mean free path, while p and ξ are the surface scattering and the grain boundary scattering parameters, respectively. The fit (blue line) reproduces the experimental data and yields $\lambda_{\mathrm{mf}} = 10 \pm 4$ nm, $p = 0.9 \pm 0.03$, $\xi = 0.6 \pm 0.2$, and $\rho_0 = 130 \pm 9$ $\mu\Omega$cm. We found that the measured resistivity was larger than 140 $\mu\Omega$cm in the thickness range of 2–30 nm, indicating that the films in this thickness range are dominated by β-Ta phase [26,44]. In addition, when we limited our fitting range to 2–30 nm (red line), the extrapolated values change to $\lambda_{\mathrm{mf}} = 7 \pm 4$ nm, $p = 0.9 \pm 0.06$, $\xi = 0.6 \pm 0.2$, and $\rho_0 = 139 \pm 13.6$ $\mu\Omega$cm. The extrapolated bulk resistivity is very close to the value of β-Ta, suggesting that β-Ta is dominant when the thickness is below 30 nm. To further confirm this, we performed XRD measurements. As shown in Fig. 3(b), Ta films with thicknesses of 20, 30, 40, and 50 nm were dominated by the tetragonal β-Ta phase since a strong peak corresponding

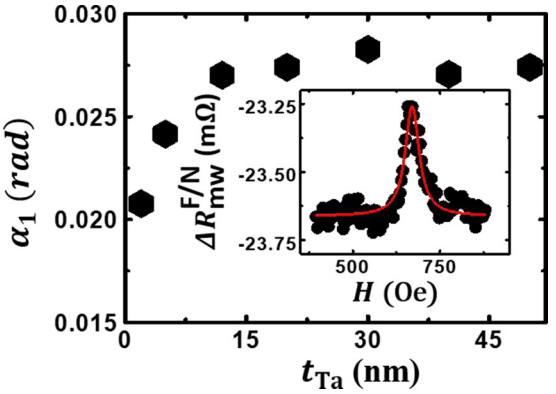

FIG. 4. In-plane precession angle as a function of Ta thickness. The inset shows a typical microwave photoresistance signal used for the estimation of the in-plane precession angle. The signal was obtained with $\alpha_0 = 90^\circ$ and $f = 10$ GHz for Ta (20)/CoFeB (10).

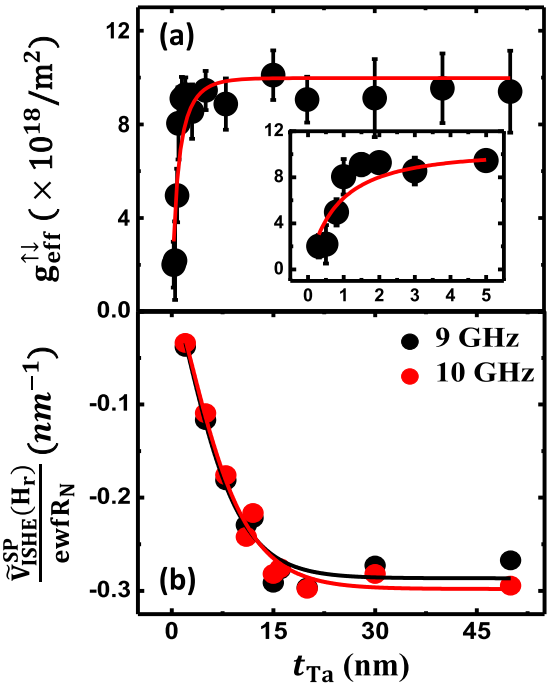

FIG. 5. (a) Ta thickness dependence of the effective spin mixing conductance. The solid line is the fit according to Eq. (1). The inset shows the effective spin mixing conductance as the function of Ta thickness in the range 0–5 nm. (b) Ta thickness dependence of ISHE signal measured at 9 GHz (black circle) and 10 GHz (red circle). The solid lines are the fits utilizing Eq. (2).

to the Bragg diffraction peak (002) of β-Ta was found. In the large-thickness region, namely at thicknesses of 40 and 50 nm, we also observed a weak peak corresponding to the (110) Bragg diffraction peak of α-Ta, in good agreement with previous findings [44]. As shown in the inserted amplified view, we did not observe any α-Ta peak for films with thickness of 30 nm and less, which is consistent with the resistivity measurements indicating films mainly in β-phase. Thus, we can conclude that our deposited Ta films are indeed dominated by the β-phase for thickness below 30 nm, and we will limit our discussion of the spin pumping induced ISHE measurements in this range.

In the following, we discuss the method for estimating the magnitude of the pumped spin current. According to the spin pumping theory [45], the pumped spin current is proportional to the product of the in- and out-of-plane precession angles. At the resonance condition, $j_s^0(H_r) \propto g_{eff}^{\uparrow\downarrow} f \alpha_1 \beta_1$, where $g_{eff}^{\uparrow\downarrow}$ is the effective spin mixing conductance parameter, and α_1, β_1 are the in- and out-of-plane precession angles at the resonance field, respectively. Therefore, an accurate characterization of the precession angles is also crucial for the estimation of the magnitude of the pumped spin current and the calculation of θ_{SH}. This crucial step, however, is ignored in many studies where it is often assumed that a given microwave power always yields the same $\vec{h}_{rf}$ in the sample. With microwave photoresistance measurements, recent studies showed that the precession angle can change when the thickness of Pd layer is varied in Py/Pd [13]. The method was originally used to study the spin rectification effect [30] and was recently adopted for a spin pumping study [12]. The validity of the method is further confirmed by Ref. [32], where different methods were compared; only this method can ensure the frequency independence of the spin Hall angle. We continued using this method to estimate α_1 and β_1 for each individual sample. Figure 4 presents t_{Ta} dependence of α_1 at $\alpha_0 = 90^\circ$ with microwaves of $f = 10$ GHz and amplitude of -18 dBm, combined with a microwave amplifier with a gain of 200. A typical microwave photoresistance measurement is shown in the inset utilizing Ta (20)/CoFeB (10) as an example. The black circles are the experimental data, and the solid red line is the fit utilizing a symmetrical Lorentzian function. The amplitude at H_r is used to calculate α_1 for each individual sample, and a t_{Ta} dependence is obtained. We found that α_1 increased with t_{Ta} up to 15 nm and then remained almost constant with further increasing t_{Ta}. The result confirms that the precession angle is indeed not a constant for different samples even when they are excited with the same input microwave power. Thus, careful measurement of the precession angles for each sample is necessary in the quantitative estimation of θ_{SH}, as we did for Ta in this study.

Damping enhancement ($\Delta\alpha = \alpha_{F/N} - \alpha_F$, where $\alpha_{F/N}$ is the total damping for F/N bilayer and α_F is the damping for a single F layer) is the main character of spin pumping [45]. It also contains information of the absorption of spin current at the interface [36,37]. Therefore, the enhancement of damping can be used to characterize the influence of the interface on the transportation of spin current. With FMR measurements, we obtain the damping parameter α by using the slope of FMR linewidth as a function of microwave frequency. Further, we can calculate the effective spin mixing conductance $g_{eff}^{\uparrow\downarrow}$ according to $g_{eff}^{\uparrow\downarrow} = (4\pi M_S t_F / g\mu_B)(\alpha_{F/N} - \alpha_F)$, where M_S is the saturate magnetization and t_F is the thickness of the FM layer. To further illustrate the interface effect, measurements with $t_{Ta} < 2$ nm were taken from a series of samples made by a wedge-shape growth technique. Figure 5(a) illustrates $g_{eff}^{\uparrow\downarrow}$ as the function of t_{Ta}. To highlight the change at $t_{Ta} < 2$ nm, we also show the amplified view in the inset for the small-thickness range. We find that $g_{eff}^{\uparrow\downarrow}$ has a fast increase when $t_{Ta} < 2$ nm and reaches a saturation value at $t_{Ta} \sim 1.5$ nm. The result is similar to that of previous study where a saturation thickness

of ∼2 nm was reported [46]. As mentioned above, we can exclude most of the unwanted spin rectification effect and obtained the ISHE signal at the special chosen geometries, namely at $\alpha_0 = 90°, 270°$. To further eliminate the residual spin rectification effect, we measured SP-ISHE and the microwave photoresistance effect at both geometries in the same setup, and redefined a normalized ISHE voltage induced by spin pumping, $\tilde{V}^{\rm SP}_{\rm ISHE}(H_{\rm r}) = [\frac{V}{\alpha_1\beta_1}|_{\alpha_0=90°} - \frac{V}{\alpha_1\beta_1}|_{\alpha_0=270°}]/2$. Together with the measured $g^{\uparrow\downarrow}_{\rm eff}$ and the Ta resistance $R_{\rm N}$ for each individual sample, we plot the thickness-dependent $\frac{\tilde{V}^{\rm SP}_{\rm ISHE}(H_{\rm r})}{ewfR_{\rm N}}$ in Fig. 5(b). The black circle and the red circle represent data obtained at frequencies of 9 and 10 GHz, respectively. All the ISHE data are negative in the thickness range that we investigated. The signal shows a decrease with increasing thickness and reaches a saturation at $t_{\rm Ta} \approx 20$ nm. Comparing with the measured $t_{\rm Ta}$-dependent $g^{\uparrow\downarrow}_{\rm eff}$ shown in Fig. 4(a), we found that two signals reach their saturation values at very different thicknesses. Namely, one is at ∼1.5 nm and the other is at ∼20 nm. This dramatic difference was also reported in the Py/Pt system [12] and Co/Pt system [35]. A possible explanation is the spin loss at the interface [35–37,47]. It suggests that the pumped pure spin current not only transmits and reflects at the F/N interface but also suffers a loss, the interface spin loss, as shown in the right panel of Fig. 1(b).

The spin loss at the interface was originally introduced in the study of current-perpendicular-to-plane (CPP) giant magnetoresistance [48,49]. Rojas-Sánchez *et al.* combined the spin diffusion model with spin pumping measurements to study the spin pumping induced ISHE in the Co/Pt system [35] to show the important role of spin memory loss at the interface. First-principles calculations confirm that a considerable part of the pumped spin current dissipates at the Py/Pt interface [50]. Zhang *et al.* also described the spin loss utilizing a parameter denoting the transparency of the interface in the investigation of the spin-charge conversion in Pt [47]. Chen and Zhang revisited spin pumping theory including spin-orbit coupling (SOC) at the interface and found a discontinuity in the spin current at the interface [37]. The interface spin loss provides a possible explanation for $g^{\uparrow\downarrow}_{\rm eff}$ and $\frac{\tilde{V}^{\rm SP}_{\rm ISHE}(H_{\rm r})}{ewfR_{\rm N}}$ having different approaches to saturation with increasing thicknesses of the nonmagnetic layer. Interestingly, the theory by Chen and Zhang only requires careful thickness-dependent measurements of $g^{\uparrow\downarrow}_{\rm eff}$ and $\frac{\tilde{V}^{\rm SP}_{\rm ISHE}(H_{\rm r})}{ewfR_{\rm N}}$ to estimate the spin loss at the interface. It does not need additional measurements for extra parameters such as the interfacial resistance.

We used this model to analyze our experimental data. For the reader's convenience, we briefly summarize the model here. The essential assumption is that every time the spin current crosses the F/N interface, it loses amplitude by a factor of δ and only $(1-\delta)J_{\rm S}$ crosses the interface [36,37,51]. Since the backflow spin current [51] has to cross the interface twice, first on the way into nonmagnetic layer and second on the way back to the ferromagnetic layer, the effective spin mixing conductance thus can be written as

$$g^{\uparrow\downarrow}_{\rm eff} = G^{\uparrow\downarrow}[1-(1-\delta)^2\varepsilon], \tag{1}$$

where $\varepsilon = G^{\uparrow\downarrow}/(G^{\uparrow\downarrow} + \frac{2}{3}k_{\rm F}^2\frac{\lambda_{\rm mf}}{\lambda_{\rm sd}}\tanh\frac{t_{\rm N}}{\lambda_{\rm sd}})$ characterizes the back-flow spin current and $k_{\rm F}$ is the Fermi vector of the N layer. The model also estimates the transmitted pure spin current and the loss at the interface to be $G^{\uparrow\downarrow}(1-\varepsilon)(1-\delta)$ and $G^{\uparrow\downarrow}(1+\varepsilon-\varepsilon\delta)\delta$, respectively. The transmitted pure spin current is converted to the charge current via ISHE. Meanwhile the lost pure spin current can also contribute an additional charge voltage via the inverse Edelstein effect [52,53]. By summing up both contributions together, the total converted charge signal can be written as

$$\frac{\tilde{V}^{\rm SP}_{\rm ISHE}(H_{\rm r})}{ewfR_{\rm N}} = G^{\uparrow\downarrow}(1-\varepsilon)(1-\delta)\theta_{\rm SH}\lambda_{\rm sd}\tanh\left(\frac{t_{\rm N}}{2\lambda_{\rm sd}}\right) + \lambda_{\rm IEE}G^{\uparrow\downarrow}(1+\varepsilon-\varepsilon\delta)\delta, \tag{2}$$

where λ_{IEE} is known as the inverse Edelstein length [36,37].

We took Eqs. (1) and (2) to fit our experimental data in the thickness range of 2–30 nm since we found that Ta is dominated by the β phase in this range. The data above 30 nm are presented only to double check that the measured effective spin mixing conductance and spin pumping induced ISHE signal reach their saturation. In the fits, we chose a literature value of $k_{\rm F} = 11.8$ nm^{-1} reported in Ref. [27]. To further minimize the number of parameters in the whole fitting process, we took two steps to fit the experimental data in Fig. 5(a) and Fig. 5(b). First, we used a fixed test value for $\lambda_{\rm mf}$ and $\lambda_{\rm sd}$ to fit $G^{\uparrow\downarrow}$ and δ for the measured $G^{\uparrow\downarrow}_{\rm eff} \sim t_{\rm N}$ data according to Eq. (1). With the extracted values of $G^{\uparrow\downarrow}$ and δ, we continued to fit $\frac{\tilde{V}^{\rm SP}_{\rm ISHE}(H_{\rm r})}{ewfR_{\rm N}} \sim t_{\rm N}$ data according to Eq. (2) to obtain $\theta_{\rm SH}$ and $\lambda_{\rm sd}$. We repeated these two fitting steps with the newly obtained $\lambda_{\rm sd}$ until a convergence was reached. We found the curves can be best fitted with $\lambda_{\rm mf} = 3.7$ nm, which lies between the error margin gives by Fuchs-Sondheimer theory (7 ± 4 nm) and is larger than that obtained via Drude model (0.64 nm). In Fig. 5(a) and its inset, the resulting fits are plotted as the red lines. It can be found that the fits reproduce the experimental data well. The fits also yield $G^{\uparrow\downarrow} = (1.17 \pm 0.07) \times 10^{19}$ m^{-2} and a small spin loss factor δ of 0.02 ± 0.02. The small spin loss is consistent with the value about 0.049 adopted for the same system by Cecot *et al.* [54] using the spin diffusion model [48]. The experimentally obtained $t_{\rm Ta}$-dependent voltage signal can also be well described by Chen and Zhang's theory as shown in Fig. 5(b), where the black and red lines represent the fits for 9 and 10 GHz, respectively. The fits yield $\theta_{\rm SH} = -0.0064 \pm 0.001$, $\lambda_{\rm sd} = 4.8 \pm 0.6$ nm, and $\lambda_{\rm IEE} = 0.06 \pm 0.09$ nm for 9 GHz; $\theta_{\rm SH} = -0.0060 \pm 0.0007$, $\lambda_{\rm sd} = 5.3 \pm 0.5$ nm, and $\lambda_{\rm IEE} = 0.06 \pm 0.07$ nm for 10 GHz. By averaging these two values, we obtained $\theta_{\rm SH} = -0.0062 \pm 0.001$ and $\lambda_{\rm sd} = 5.1 \pm 0.6$ nm for β-phase dominated Ta. We also obtained $\lambda_{\rm IEE} = 0.06 \pm 0.08$ nm which is close to zero. The interface spin loss for CoFeB-Ta is tiny, i.e., the interface is highly transparent for spin current, indicating that the interface Rashba spin-orbit interaction is not large. In addition, The value of $\lambda_{\rm IEE}$ not only depends the Rashba spin-orbit interaction, but also is influenced by the interface disorder [36]. Since our bilayers are fabricated by sputtering, interfacial disorder is expected and the inverse Edelstein effect could be strongly suppressed

resulting in the small value of λ_{IEE}. If the interface is sharper, for instance, from layer-by-layer growth by molecular beam epitaxy, we would expect a larger λ_{IEE} value in that case.

In the following, we make a brief comparison of our data with previous studies. Interestingly, we found our measured spin Hall angle and spin diffusion length are in good agreement with those extracted from lateral spin valve geometry in Ref. [55], where $\theta_{SH} = -0.008 \pm 0.002$ and $\lambda_{sd} = 3 \pm 0.4$ nm were reported. Our results are also in good agreement with the values of $G^{\uparrow\downarrow} = 1.4 \times 10^{19}$ m^{-2}, $\theta_{SH} = -0.005$, and $\lambda_{sd} = 2.5$ nm reported in Ref. [25] even though the authors made the assumption that the relative ratio between the symmetric/antisymmetric signals in the spin rectification effect are the same for CoFeB and CoFeB/Ta. Interestingly, the same authors refined the value of spin Hall angle to -0.02 ± 0.0007 but they assumed the symmetrical component of the measured signal originates from the SP-ISHE only [28]. A similar system was also studied by Jamali *et al.* [24] using spin pumping, and a different value of spin Hall angle, -0.014, was reported. The difference may be due to the fact that their sample was annealed at a temperature above 200 °C while our samples are grown at room temperature and without any annealing. Evidence of the difference in samples between our study and that of Jamali *et al.* [24] can also be observed in the significantly different effective spin mixing conductance. The spin Hall angle of Ta in Ta/CoFeB was also studied by spin transfer torque FMR, and much larger values were reported. Generally, the spin Hall angle obtained by spin transfer torque FMR is about one order of magnitude larger than the one measured by spin pumping, as reported for Pt as well [20]. The reason is not well understood at the present stage and deserves further investigation.

In summary, we studied the dc electron transport and spin pumping induced ISHE in an important class of Ta thin films that play a crucial role in spin pumping current transport and spin torque devices. Using t_{Ta}-dependent resistivity and XRD measurements we found that, in the region of interest for our study, $2 < t_{Ta} < 30$ nm, the dominant structure of Ta is β phase. Through t_{Ta}-dependent microwave photoresistance measurements, we found that the precession angles are different for films with different t_{Ta} even with the same input microwave power. Thus, to quantify the pumped pure spin current, precession angle characterization for each individual sample is needed. Together with t_{Ta} -dependent effective spin mixing conductance and ISHE voltage measurements as well as the interface spin loss described by Chen and Zhang [36,37], we obtained consistent values of $\theta_{SH} = -0.0062 \pm 0.001$ and $\lambda_{sd} = 5.1 \pm 0.6$ nm at two different microwave frequencies of 9 and 10 GHz.

This work was supported by the National Key R&D Program of China (Grants No. 2017YFA0303202 and No. 2018YFA0306004), the National Natural Science Foundation of China (Grants No. 51571109, No. 11734006, No. 51601087, No. 11374145, and No. 51471085), the Natural Science Foundation of Jiangsu Province (Grant No. BK20150565), and the Fundamental Research Funds for the Central Universities (Grant No. 14380078). M.W. was supported by the SHINES, an Energy Frontier Research Center funded by the U.S. Department of Energy (SC0012670), and the U.S. National Science Foundation (EFMA-1641989, DMR-1407962). P. O. and B. H. were supported by the Natural Sciences and Engineering Research Council of Canada (NSERC).

[1] S. A. Wolf, D. D. Awschalom, R. A. Buhrman, J. M. Daughton, S. von Molnár, M. L. Roukes, A. Y. Chtchelkanova, and D. M. Treger, Science **294**, 1488 (2001).
[2] Y. Tserkovnyak, A. Brataas, G. E. Bauer, and B. I. Halperin, Rev. Mod. Phys. **77**, 1375 (2005).
[3] S. D. Bader, Rev. Mod. Phys. **78**, 1 (2006).
[4] S. Bader and S. Parkin, Annu. Rev. Condens. Matter Phys. **1**, 71 (2010).
[5] J. Sinova, S. O. Valenzuela, J. Wunderlich, C. Back, and T. Jungwirth, Rev. Mod. Phys. **87**, 1213 (2015).
[6] S. Murakami, N. Nagaosa, and S.-C. Zhang, Science **301**, 1348 (2003).
[7] *Spin Current*, edited by S. Maekawa, SO Valenzuela, E. Saitoh, and T. Kimura (Oxford University Press, Oxford, 2012).
[8] S. Maekawa, H. Adachi, K.-i. Uchida, J. i. Ieda, and E. Saitoh, J. Phys. Soc. Jpn. **82**, 102002 (2013).
[9] S. O. Valenzuela and M. Tinkham, Nature (Lonond) **442**, 176 (2006).
[10] E. Saitoh, M. Ueda, H. Miyajima, and G. Tatara, Appl. Phys. Lett. **88**, 182509 (2006).
[11] O. Mosendz, J. E. Pearson, F. Y. Fradin, G. E.W. Bauer, S. D. Bader, and A. Hoffmann, Phys. Rev. Lett. **104**, 046601 (2010).
[12] Z. Feng *et al.*, Phys. Rev. B **85**, 214423 (2012).
[13] X. Tao, Z. Feng, B. Miao, L. Sun, B. You, D. Wu, J. Du, W. Zhang, and H. Ding, J. Appl. Phys. **115**, 17C504 (2014).
[14] B. F. Miao, S. Y. Huang, D. Qu, and C. L. Chien, Phys. Rev. Lett. **111**, 066602 (2013).
[15] L. Liu, T. Moriyama, D. C. Ralph, and R. A. Buhrman, Phys. Rev. Lett. **106**, 036601 (2011).
[16] S. W. Jiang, S. Liu, P. Wang, Z. Z. Luan, X. D. Tao, H. F. Ding, and D. Wu, Phys. Rev. Lett. **115**, 086601 (2015).
[17] T. Tanaka, H. Kontani, M. Naito, T. Naito, D. S. Hirashima, K. Yamada, and J. Inoue, Phys. Rev. B **77**, 165117 (2008).
[18] Y. Niimi, Y. Kawanishi, D. H. Wei, C. Deranlot, H. X. Yang, M. Chshiev, T. Valet, A. Fert, and Y. Otani, Phys. Rev. Lett. **109**, 156602 (2012).
[19] H. L. Wang, C. H. Du, Y. Pu, R. Adur, P. C. Hammel, and F. Y. Yang, Phys. Rev. Lett. **112**, 197201 (2014).
[20] L. Liu, C.-F. Pai, Y. Li, H. Tseng, D. Ralph, and R. Buhrman, Science **336**, 555 (2012).
[21] M. Morota, Y. Niimi, K. Ohnishi, D. H. Wei, T. Tanaka, H. Kontani, T. Kimura, and Y. Otani, Phys. Rev. B **83**, 174405 (2011).
[22] P. Deorani and H. Yang, Appl. Phys. Lett. **103**, 232408 (2013).
[23] C. Hahn, G. de Loubens, O. Klein, M. Viret, V. V. Naletov, and J. Ben Youssef, Phys. Rev. B **87**, 174417 (2013).
[24] M. Jamali, A. Klemm, and J.-P. Wang, Appl. Phys. Lett. **103**, 252409 (2013).
[25] D.-J. Kim, S.-I. Kim, S.-Y. Park, K.-D. Lee, and B.-G. Park, Curr. Appl. Phys. **14**, 1344 (2014).

[26] D. Qu, S. Y. Huang, B. F. Miao, S. X. Huang, and C. L. Chien, Phys. Rev. B **89**, 140407 (2014).
[27] G. Allen, S. Manipatruni, D. E. Nikonov, M. Doczy, and I. A. Young, Phys. Rev. B **91**, 144412 (2015).
[28] S.-I. Kim, D.-J. Kim, M.-S. Seo, B.-G. Park, and S.-Y. Park, Appl. Phys. Lett. **106**, 032409 (2015).
[29] L. Bai, Z. Feng, P. Hyde, H. Ding, and C.-M. Hu, Appl. Phys. Lett. **102**, 242402 (2013).
[30] N. Mecking, Y. S. Gui, and C.-M. Hu, Phys. Rev. B **76**, 224430 (2007).
[31] A. Azevedo, L. H. Vilela-Leão, R. L. Rodríguez-Suárez, A. L. Santos, and S. M. Rezende, Phys. Rev. B **83**, 144402 (2011).
[32] S. Gupta, R. Medwal, D. Kodama, K. Kondou, Y. Otani, and Y. Fukuma, Appl. Phys. Lett. **110**, 022404 (2017).
[33] M. Kavand, C. Zhang, D. Sun, H. Malissa, Z. V. Vardeny, and C. Boehme, Phys. Rev. B **95**, 161406(R) (2017).
[34] J. Bass and W. P. Pratt Jr, J. Phys. Condens. Matter. **19**, 183201 (2007).
[35] J.-C. Rojas-Sánchez, N. Reyren, P. Laczkowski, W. Savero, J.-P. Attané, C. Deranlot, M. Jamet, J.-M. George, L. Vila, and H. Jaffrés, Phys. Rev. Lett. **112**, 106602 (2014).
[36] K. Chen and S. Zhang, Phys. Rev. Lett. **114**, 126602 (2015).
[37] K. Chen and S. Zhang, IEEE. Magn. Lett. **6**, 1 (2015).
[38] M. Obstbaum, M. Härtinger, H. G. Bauer, T. Meier, F. Swientek, C. H. Back, and G. Woltersdorf, Phys. Rev. B **89**, 060407(R) (2014).
[39] M. H. Read and C. Altman, Appl. Phys. Lett. **7**, 51 (1965).
[40] J. J. Senkevich, T. Karabacak, D.-L. Bae, and T. S. Cale, J. Vac. Sci. Technol. B **24**, 534 (2006).
[41] M. Grosser and U. Schmid, Thin Solid Films **517**, 4493 (2009).
[42] M. Shiojiri, S. Shinkai, K. Sasaki, H. Yanagisawa, and Y. Abe, Jpn. J. Appl. Phys. **42**, 4499 (2003).
[43] P. Fan, K. Yi, J.-D. Shao, and Z.-X. Fan, J. Appl. Phys. **95**, 2527 (2004).
[44] E. Montoya, P. Omelchenko, C. Coutts, N. R. Lee-Hone, R. Hübner, D. Broun, B. Heinrich, and E. Girt, Phys. Rev. B **94**, 054416 (2016).
[45] Y. Tserkovnyak, A. Brataas, and G. E. W. Bauer, Phys. Rev. Lett. **88**, 117601 (2002).
[46] A. Conca, B. Heinz, M. R. Schweizer, S. Keller, E. T. Papaioannou, and B. Hillebrands, Phys. Rev. B **95**, 174426 (2017).
[47] W. Zhang, W. Han, X. Jiang, S.-H. Yang, and S. S. Parkin, Nat. Phys. **11**, 496 (2015).
[48] A. Fert and S.-F. Lee, Phys. Rev. B **53**, 6554 (1996).
[49] D. V. Baxter, S. Steenwyk, J. Bass, and W. Pratt Jr, J. Appl. Phys. **85**, 4545 (1999).
[50] Y. Liu, Z. Yuan, R. J. H. Wesselink, A. A. Starikov, and P. J. Kelly, Phys. Rev. Lett. **113**, 207202 (2014).
[51] H. J. Jiao and G. E. W. Bauer, Phys. Rev. Lett. **110**, 217602 (2013).
[52] G. Bihlmayer, Y. M. Koroteev, P. Echenique, E. Chulkov, and S. Blügel, Surf. Sci. **600**, 3888 (2006).
[53] J. R. Sánchez, L. Vila, G. Desfonds, S. Gambarelli, J. Attané, J. De Teresa, C. Magén, and A. Fert, Nat. Commun. **4**, 2944 (2013).
[54] M. Cecot *et al.*, Sci. Rep. **7**, 968 (2017).
[55] Y. Niimi, H. Suzuki, Y. Kawanishi, Y. Omori, T. Valet, A. Fert, and Y. Otani, Phys. Rev. B **89**, 054401 (2014).